The role of steam treatment on the structure, purity and length distribution of multi-walled carbon nanotubes

Reference:

Cabana Laura, Ke Xiaoxing, Kepić Dejan, Oro-Solé Judith, Tobías-Rossell Ester, van Tendeloo Gustaaf, Tobias Gerard.- The role of steam treatment on the structure, purity and length distribution of multi-walled carbon nanotubes
Carbon - ISSN 0008-6223 - 93(2015), p. 1059-1067
DOI: http://dx.doi.org/doi:10.1016/j.carbon.2015.06.027

The role of steam treatment on the structure, purity and length distribution of multi-walled carbon nanotubes

Laura Cabana[1], Xiaoxing Ke[2], Dejan Kepić[1,3], Judith Oro-Solé[1], Ester Tobías-Rossell[4], Gustaaf Van Tendeloo[2], Gerard Tobias[1*]

[1]*Institut de Ciència de Materials de Barcelona (ICMAB-CSIC), Campus UAB, 08193 Bellaterra, Barcelona, Spain.*

[2]*Electron Microscopy for Materials Science (EMAT), University of Antwerp, Groenenborgerlaan 171, B-2020, Antwerp, Belgium.*

[3]*Vinča Institute of Nuclear Sciences, University of Belgrade, Mike Alasa 12-14, Belgrade, Serbia*

[4]*Escola Universitària de Ciències de la Salut de Manresa, Universitat de Vic-Universitat Central de Catalunya, Av. Universitària 4-6, 08242 Manresa, Barcelona, Spain*

*Corresponding author. E-mail: gerard.tobias@icmab.es (Gerard Tobias); Tel. +34 93 580 1853

Abstract

Purification and shortening of carbon nanotubes have attracted a great deal of attention to increase the biocompatibility and performance of the material in several applications. Steam treatment has been employed to afford both purification and shortening of multi-walled carbon nanotubes (MWCNTs). Steam removes the amorphous carbon and the graphitic particles that sheath catalytic nanoparticles, facilitating their removal by a subsequent acidic wash. The amount of metal impurities can be reduced in this manner below 0.01 wt.%. The length distribution of MWCNTs after different steam treatment times (from 1 h to 15 h) was assessed by box plot analysis of the electron microscopy data. Samples with a median length of 0.57 μm have been prepared with the reported methodology whilst preserving the integrity of the tubular wall structure.

1. Introduction

Bulk synthesis of carbon nanotubes (CNTs) results in samples that contain several impurities, namely amorphous carbon, graphitic particles in the form of fullerenes or nano-onions, and metal nanoparticles when employed for the catalytic growth of CNTs. The presence of these impurities is detrimental for further processing and application of CNTs. Metal nanoparticles not only might induce cytotoxicity [1-3] but can also dominate the electrochemical response of the material [4] along with graphitic particles [5-7]. On the other hand, the presence of amorphous carbon alter the adhesion properties of the nanotubes [8] and might lead to the formation of oxidation debris preventing the sidewall functionalization of CNTs [9]. A wide range of purification strategies have been employed to remove these side products; liquid phase treatments in oxidising acidic conditions being the most widely used. For instance, the combination of HCl and HNO_3 has been shown to simultaneous remove non-nanotube carbon material along with metal and metal oxide nanoparticles present in samples of multi-walled carbon nanotubes (MWCNTs) [10], leading to purities above 96 wt.% [11]. Other liquid phases treatments for the purification of MWCNTs involve the use of hydrogen peroxide, followed by an HCl wash [12] or chlorine and ammonia water [13]. Gas phase reactions not only reduce the amount of chemical waste but also present some advantages compared to liquid phase treatments [14, 15]. Gas phase purification of MWCNTs commonly involve air [16] but steam [17], carbon dioxide [18], chlorine [19], hydrogen [20], and plasma-thermal purification [21] have also been explored. Purification studies on as-produced single-walled carbon nanotubes (SWCNTs) have revealed that air-oxidation can remove the associated impurities while inflicting considerably less damage than oxidising acid-treatment, and avoid the formation of oxidation debris [15]. Unlike liquid phase oxidation the gas phase process preferentially

oxidizes SWCNTs without introducing sidewall defects [22]. Oxygen reacts with carbon in a fast manner, above a given temperature. Therefore when air is employed for the purification of CNT samples a careful optimization of the temperature and treatment time is necessary from batch to batch to avoid the complete oxidation and loss of the carbon material. Steam, being a milder oxidizing agent, allows a better control of the purification with reactions with as-produced SWCNTs that can last for several hours [23]. Steam has been combined with oxidizing acid treatments for the purification of cloth-like soot SWCNTs from arc discharge [24], because steam can efficiently remove the functionalities introduced by the acid treatment [17]. Steam treatment has also been used for the controlled etching of multi-walled carbon nanotubes decorated with iron nanoparticles [25]. The etching occurred only at the interface between the iron nanoparticles and the nanotubes. Steam purified carbon nanotubes are being employed for a wide range of applications such as lithium-ion batteries [26], supercapacitors [27, 28], ceramic composites [29], templated growth of novel structures [30], biomedical applications [31, 32] or even for the formation of graphene by unzipping steam purified nanotubes [28]. Furthermore, initial studies reveal that short SWCNTs can be obtained after prolonged steam treatment [23]. Short CNTs have an increased biocompatibility and are desired for a wide range of applications including biomedicine [33, 34], sensors [35], membranes [36] and electrode materials [37]. As such, a toolbox of cutting and shortening strategies is nowadays available including ball milling [38], lithography [39], fluorination [40] and oxidation [41].

From just the few examples noted above, it becomes clear that there is a growing interest in the use of steam for the post-synthesis processing of CNT material. Steam is actually widely employed as an oxidative additive during the synthesis of carbon

nanotubes by chemical vapor deposition (CVD). When steam is added into the reactor, not only the formation of amorphous carbon is suppressed, but also the activity and lifetime of the catalysts are greatly improved [42, 43]. Thus, using steam is possible to synthesize high-purity CNTs and is an efficient additive for the supergrowth of aligned SWCNTs [44]. However, the role of steam onto the post-synthesis treatment of MWCNT samples has barely been studied. As in the case of their SWCNT counterparts, it has been shown that steam removes the amorphous carbon and opens the ends of MWCNTs [17]. Here we report for the first time on the effect of the steam treatment on the length distribution of MWCNTs, wall structure, and residual inorganic content of the samples.

2. Experimental and methods

Chemical vapour deposition Elicarb® MWCNTs from Thomas Swan & Co. Ltd. were supplied as dry powder, with an average diameter of 10-12 nm (value provided by the company). The samples contained amorphous carbon, graphitic particles (carbonaceous crystalline materials having few graphitic layers) and inorganic particles. CoMoCAT® CVD MWCNTs from SouthWest NanoTechnologies were purchased from Sigma-Aldrich as dry powder. The CoMoCAT® MWCNTs have an average diameter of 10 nm ± 1 nm and a purity of ≥98% carbon basis (values provided by the company). The as-received material was finely grounded with an agate mortar and pestle and spread on the center part inside a silica tube of 5 cm in diameter. The silica tube, opened at both ends, was then placed into the alumina tube of the furnace and purged with argon (150 mL min^{-1}) for 2 h to allow the complete removal of air. Steam was introduced by flowing the incoming argon through a bubbler with hot water (98 ºC). Therefore, a mixture of Ar/steam gets in contact with the sample. The temperature of the furnace was then

increased up to 900 ºC and dwelled for different periods of time between 1 to 15 h. The sample was next treated with 6 M HCl to remove catalytic particles. Finally the powder was collected by filtration through a 0.2 μm polycarbonate membrane and washed with distilled water until the pH of the filtrate was neutral.

Thermogravimetric analysis (TGA) were performed on Netzsch instrument, model STA 449 F1 Jupiter® (Elicarb® MWCNTs) or in a Mettler Toledo TGA/SDTA851e/SF/1100 (CoMoCAT® MWCNTs). Experiments were conducted under a flow of air at a heating rate of 10 ºC min^{-1} up to 950 ºC. To examine the stability of as-received Fe-growth MWCNTs, TGA was performed on SETARAM Setsys Evolution instrument. Sample was heated up to 1100 °C with a heating rate of 10 °C min^{-1} under Ar/steam flow (190 mL min^{-1} of argon and 2 g h^{-1} of steam).

Magnetic measurements were done in a Superconducting Quantum Interference Device (SQUID) magnetometer (LOT-QuantumDesign Iberia). A diamagnetic gelatine capsule was filled with 3-4 mg of sample. Data was acquired with an applied field from -50.000 Oe to +50.000 Oe at 10 K to obtain the hysteresis loops. The sample holder contribution was subtracted in all the measurements.

Raman spectra were recorded with a LabRam HR 800 Raman spectrometer, Jobin Yvon® equipped with a microscope, through a 100-fold magnification objective. A 20 mW He-Ne red laser (633 nm) and - Ar^{+} green laser (514 nm) were used. The spectra were recorded from 100 to 2000 cm^{-1}. The abscissa was calibrated with a silicon standard. Samples for Raman were prepared by sonicating the material with 2-propanol, in an ultrasonic power bath. Afterwards, these were drop dried onto a glass substrate,

building up a film of the material. To check homogeneity of the samples, three spectra at different spots on the sample were recorded. Spectra were fitted using OriginPro 8 software. Each spectrum was fitted with one Gaussian and four Lorentzian functions until satisfactory fitting criteria.

Elemental Analysis was conducted with an elemental analyzer EA 1108 Instrument and a microbalance Mettler Toledo MX5. For the measurement, 1 mg of sample was weighed and a mixture of vanadium pentoxide and tin was added to ease the combustion. Sulfanilamide was used as a pattern.

XPS were acquired with a Kratos AXIS ultra DLD spectrometer with an Al Kα X ray font and a power of 120 W. Samples were measured as dry powder. Survey-scan was conducted with a Pass Energy of 160 eV and high resolution scans at a Pass Energy of 20 eV. Hybrid-slot lens mode was employed, with an area of analysis of 700 x 300 microns.

Low magnification TEM images were obtained using a JEOL 1210 and operating at 120 kV. HRTEM images were acquired using an FEI Tecnai G2 microscope operating at 200 kV. TEM and HRTEM samples were prepared by dispersing a small amount of powder in absolute ethanol and sonicated in an ultrasonic power bath. Afterwards, the dispersion was drop dried onto a lacey carbon TEM grid.

3. Results and discussion

The reactivity of MWCNTs towards steam was assessed by TGA analysis of as-received Elicarb® Fe-grown MWCNTs under Ar/steam flow (Figure 1). As it can be

seen, MWCNTs present an excellent stability in the presence of steam until about ~900 ºC were the sample starts to oxidize. Therefore, all the subsequent treatments were performed at 900 °C.

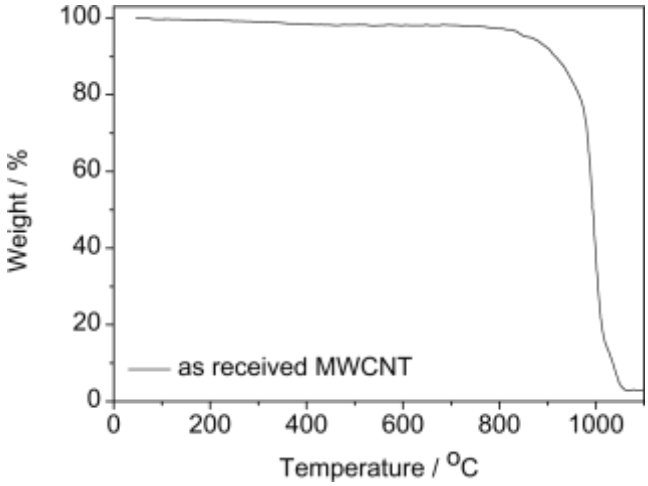

Figure 1. TGA of as-received Fe-growth CVD MWCNTs under Ar/steam flow.

Thermogravimetric analysis (TGA) under flowing air was used to assess the amount of solid residue in both as-received and steam purified samples for different periods of time, namely 1 h, 1.5 h, 2 h, 2.5 h, 5 h, 10 h and 15 h (Figure 2a). All the samples were treated with HCl before TGA measurements. Taking into account that all carbon species are oxidized to carbon dioxide, the residue from the TGA analysis must correspond to inorganic impurities from the synthesis of the nanotubes. Compared to as-received material, which contains 2.8 wt.% of inorganic solid residue, a decrease is observed up to 1.5 h of steam treatment, down to 0.5 wt.%. Longer treatments result in an increase of the inorganic content which levels off at about 1.9 wt.% for prolonged treatments (10-15 h). The solid residue obtained after the thermogravimetric analysis of the samples in air is typically attributed to the oxidation of the metal employed for the growth of the CNTs. Therefore, in the present case the residue would correspond to iron oxide (Fe_2O_3) since iron is used for the synthesis of the nanotubes. The amount of iron would then be

2.0 wt.% (as-made), 0.4 wt.% (1.5 h steam) and 1.3 wt.% (10 h). To independently assess the amount of metal content in the samples we performed magnetic measurements which have been shown to be the most accurate statistical method for quality control of CNTs [45]. Contrary to TGA, magnetic measurements are non-destructive and preserve the sample. Figure 2b presents the hysteresis loops of both as-received MWCNTs and after 1.5 h steam purification followed by HCl treatment. The as-received MWCNTs present a clear ferromagnetic behaviour superposed on a paramagnetic contribution, whereas in the purified sample a weak diamagnetic response from the holder starts to prevail. This illustrates a dramatic decrease in the amount of metal catalyst present in the sample. The saturation magnetization (M_S) of the samples after removing the linear background is 2.19 emu·g_{sample}^{-1} for the as-received material and 0.049 emu·g_{sample}^{-1} for the purified sample. Considering that the nature of the catalyst particles is pure Fe, and with iron having a bulk saturation magnetization of 221.7 emu·g^{-1} [46], the amount of metal catalyst in samples would be 0.99 wt.% for the as-received material and 0.022 wt.% for the 1.5 h steam purified sample. In contrast to their SWCNT counterparts where both TGA and SQUID revealed the same amount of catalytic impurities [23], the quantity of Fe assessed by magnetic measurements in the steam purified MWCNTs results to be an order of magnitude lower than that obtained by TGA. The same trend occurs after a prolonged 10 h steam treatment where a 0.007 wt.% of Fe is determined by SQUID measurements (0.016 emu·g_{sample}^{-1}) in contrast to a 1.3 wt.% Fe as per TGA. If the nature of the impurities present in the sample were iron oxide or iron carbide, with bulk $M_S(\gamma\text{-}Fe_2O_3)$ = 87 emu·g^{-1}; $M_S(Fe_3O_4)$ = 92 emu·g^{-1} and $M_S(Fe_3C)$ = 140 emu·g^{-1} [46], then the observed saturation magnetization after 10 h treatment would correspond to about 0.018 wt.% of iron oxide and 0.011 wt.% of iron carbide; still well below the inorganic residue observed by TGA. The observed

differences between TGA and SQUID determination of the catalytic impurities can not only arise from the fact that the M_S values of nanoparticles are typically smaller than that of the bulk material [47]. Therefore, we performed XPS analysis of the 10 h steam treated sample to determine the presence of any other inorganic species. Whereas the amount of iron was below the detection limit of this technique, an aluminium peak is clearly visible (Figure S1). Most likely aluminium is present in the sample in the oxide form as alumina, a commonly employed refractory material for high temperature syntheses. The presence of alumina impurities would indeed contribute to the TGA residue but not to the SQUID analysis, and accounts for the differences observed between both methods. Table 1 summarizes the inorganic content of representative samples. The presence of alumina in the samples becomes more visible after prolonged treatments because the carbon content diminishes with time due to its continuous removal by steam. The steam treatment followed by HCl wash is indeed an efficient approach for the removal of catalytic particles reaching levels below 0.01 wt.% Fe. The catalytic particles present in the as-received CNTs are sheathed by graphitic layers that are difficult to be oxidized even under strong acidic conditions [48]. Steam reacts with these graphitic shells leaving the metal particles exposed and susceptible to be dissolved by HCl wash. The very low residual amount of iron particles after the steam and HCl treatments makes the whole range of steam purified samples interesting for further application.

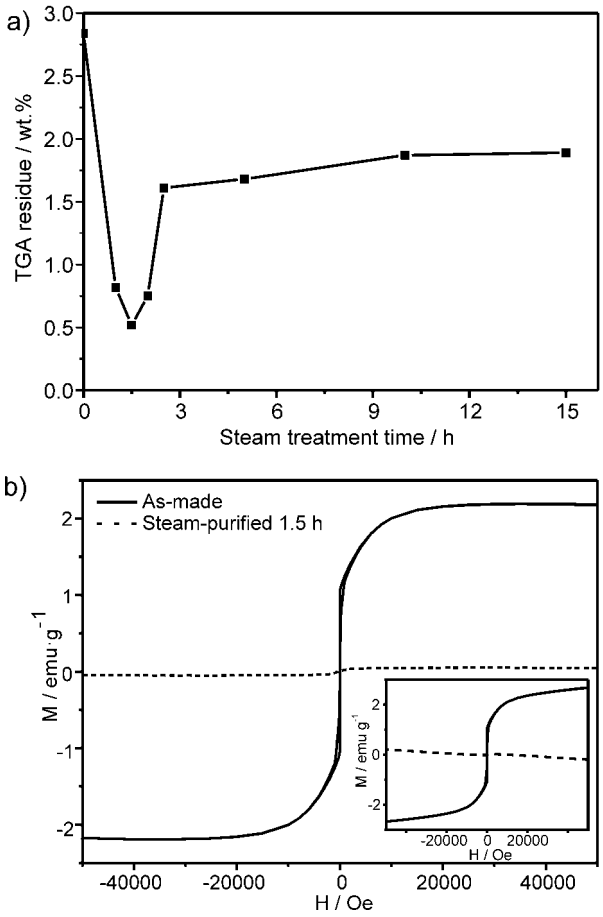

Figure 2. TGA and SQUID analysis of as-received and steam purified MWCNTs. a) Amount of residue present in the MWCNTs before (0 h) and after steam treatment (1 h up to 15 h) followed by an HCl wash, determined from TGA. b) Hysteresis loops at 10 K for as-made MWCNTs and 1.5 h steam and HCl purified MWCNTs, after linear substraction. Raw data are presented in the inset.

Sample	TGA residue (wt.%)	Fe (wt.%) SQUID	Al_2O_3 (wt.%)
as-made	2.84	0.99	1.42
1.5 h	0.52	0.022	0.48
10 h	1.87	0.007	1.86
15 h	1.89	0.013	1.87

Table 1. Inorganic impurities present in as-received and steam treated samples (after HCl wash) as determined by SQUID (wt.% Fe) and TGA. The Al_2O_3 content has been

calculated by subtraction of the wt.% of Fe_2O_3 (product of the oxidation of Fe during the TGA analysis) from the total TGA residue.

Both the amount of inorganic particles and amorphous carbon present in the samples of CNTs can influence the onset of the combustion temperature observed by TGA. Samples with a higher amount of inorganic material, such as metal nanoparticles, start to oxidize at lower temperatures [49, 50]. The same trend is also observed when amorphous carbon is present because it is more easily oxidized than carbon nanotubes [51]. In agreement, the onset of combustion of all the purified samples is higher than that of raw material (Figure S2), showing the higher quality of the steam-treated nanotubes. For the ease of comparison, TGA data of the sample holding the lowest residual content (1.5 h steam) along with the data for the as-received material are shown in Figure 3. Whereas the as-received material presents an onset of combustion at 571 ºC, an increase of 63 ºC up to 634 ºC is observed for the purified material. A detailed analysis of the shape of the TGA curve via the 1st derivative (inset) indicates two distinctive peaks for the as-received material: the first one at about 608 ºC can be assigned to the combustion of amorphous carbon and the second one at about 642 ºC can be attributed to the oxidation of carbon nanotubes [51]. Accordingly, the 1st derivative of the steam purified sample presents a single peak indicating a higher homogeneity and the successful removal of the amorphous carbon during the steam treatment.

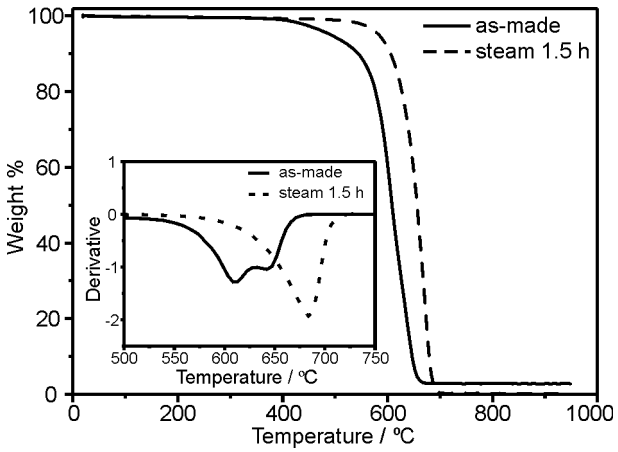

Figure 3. TGA curves in air and 1st derivative (inset) of as-received and 1.5 h steam and HCl purified MWCNTs.

In order to confirm that the steam purification was not dependent on the source of MWCNTs, CoMoCAT® MWCNTs were steam treated, followed by an HCl wash. Since the reactivity towards steam of CoMoCAT® MWCNTs might differ from that of Elicarb® Fe-grown MWCNTs, both the temperature and time of steam treatment should be optimized. Even small differences in reactivity can be encountered from batch to batch samples of a given supplier. Nevertheless, as a first approximation we employed the experimental conditions that led to the lowest amount of solid residue on Elicarb® MWCNTs (1.5 h at 900ºC). As it can be seen in Figure 4, the steam treated sample presents a higher onset of the combustion temperature compared to the as-received CoMoCAT® MWCNTs, indicating the removal of the amorphous carbon by the steam treatment. In agreement with the Fe-grown MWCNTs, a decrease in the solid residue is also observed for the steam treated CoMoCAT® MWCNTs, from 0.2 wt.% in the as-received material down to 0.004 wt.% for the steam purified sample. SQUID data also reveals a dramatic decrease in the content of magnetic catalytic particles in the sample, from a M_S of 0.57 emu·g_{sample}^{-1} in the non-treated sample down to a M_S of 0.028 emu·g_{sample}^{-1} for the purified MWCNTs.

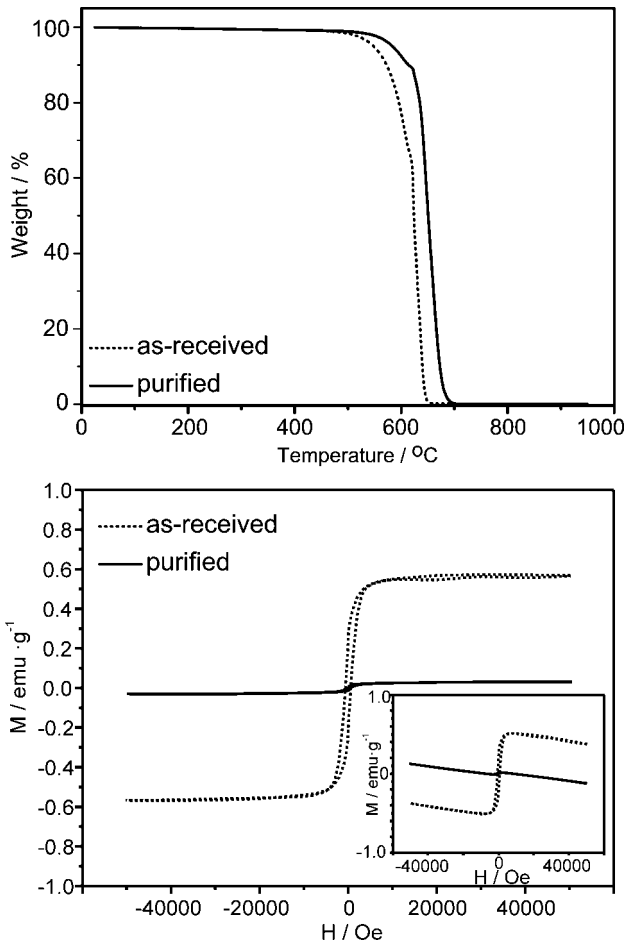

Figure 4. a) TGA curves in air and b) hysteresis loops at 10 K, of as-received and 1.5h steam and HCl purified CoMoCAT® MWCNTs.

We next investigated the effect of the steam treatment time on the length distribution of the MWCNTs. We focused on the Fe-growth MWCNTs for this and subsequent studies. For comparison we analysed the as-received material, the sample presenting the lowest amount of solid residue (1.5 h steam), and three additional samples with longer steam treatments (5 h, 10 h and 15 h). Visual inspection of the low magnification transmission electron microscopy (TEM) images presented in Figure 5 reveals a marked decrease of the MWCNTs' length with increased steam treatment time. Note that images are presented at different scales to allow observing the entire MWCNTs and contain a large amount of nanotubes for ease of inspection. We observed that steam shortened

nanotubes presented a larger amount of bundles than their long counterparts, and were more difficult to disperse. For each sample, the length of about 175 individual nanotubes was measured to quantitatively assess the decrease (Figure S3), and the results are presented as histograms in the figure. Since the samples present a non-symmetric length distribution it is not possible to determine an average mean length and a box plot analysis was performed (Figure 6, Table S1). An initial inspection of the box plot indicates a similar degree of outliers/faroutliers in all the samples, indicating that all the samples present a small amount of nanotubes that have a much longer length than the majority of the nanotubes present in each of the samples. Both as-received (0 h treatment) and 1.5 h steam treated MWCNTs are statistically similar and therefore this treatment can be employed to purify the as-received material without a significant alteration on the length distribution of the sample. As-received MWCNTs contain a high fraction of long nanotubes, with 32.2 % above 2.5 μm and a median length of 1.9 μm. When steam purification is carried out for a prolonged time, not only the length of the resulting MWCNTs is extremely diminished but also a much narrower length distribution is observed. For instance after 10 h most of the nanotubes are shorter than 2.07 μm (maximum adjacent observation, Table S1) and a median length of 0.58 μm is achieved for MWCNT samples treated with steam for 15 h. Therefore the length of the MWCNTs can be easily modulated by applying a given steam treatment time.

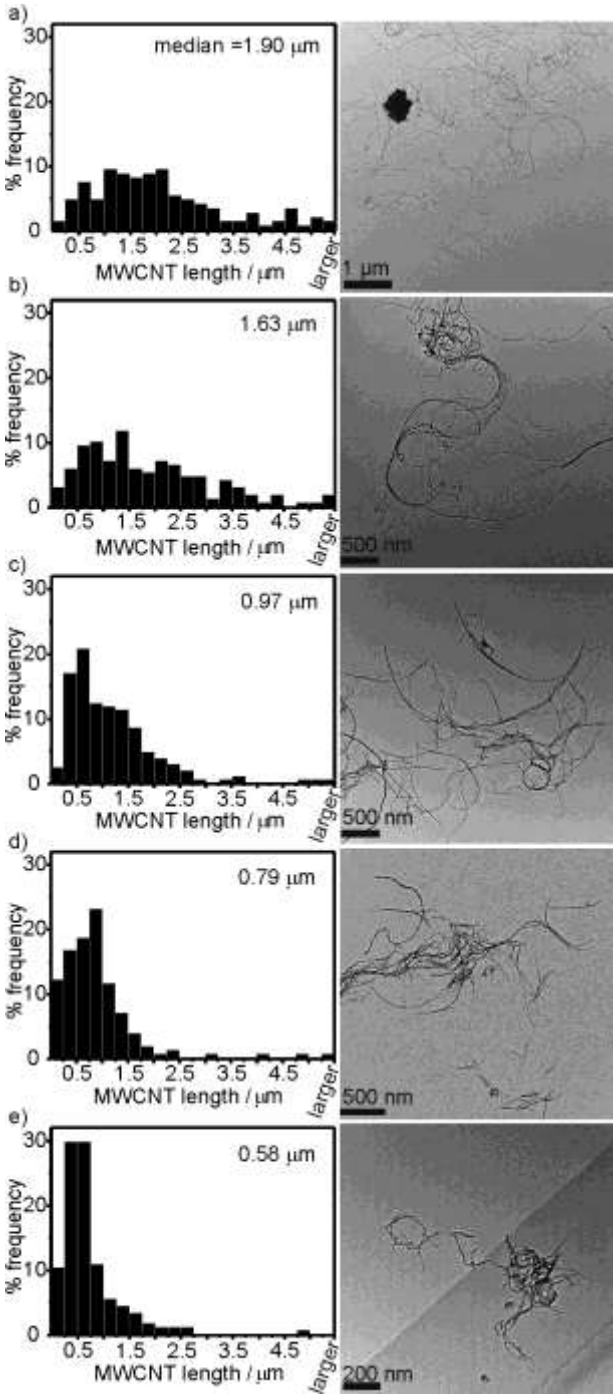

Figure 5. Low magnification TEM images and length distribution histograms of a) as-received MWCNTs, b) steam-treated MWCNTs for 1.5 h, c) 5 h, d) 10 h and e) 15h. All samples have undergone an HCl wash. Note that image magnification is different for each image to make visible the whole MWCNTs.

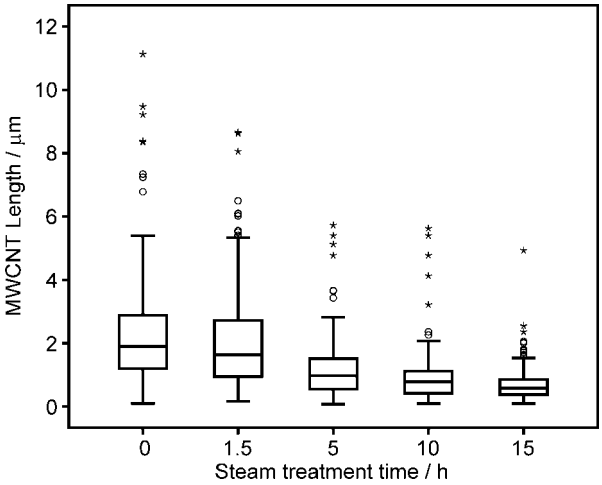

Figure 6. Box plot analysis of the as-received MWCNTs (0 h) and steam-treated MWCNTs for 1.5 h, 5 h, 10 h and 15h. All samples have undergone an HCl wash. Empty circles indicate outliers and asterisks faroutliers in the samples.

Most shortening and cutting strategies take place via a progressive introduction of defects/functionalities into the wall structure until a complete cutting is achieved [52, 53]. From the TGA curves of the steam treated samples it becomes clear that this is not the case for the steam shortened nanotubes. All the samples are completely stable under air until their complete combustion above 500 ºC (Figure S2). To determine the amount of functional groups, if any, on the samples we performed both elemental analysis and X-ray photoelectron spectroscopy (XPS). Any functionality derived from the steam treatment should contain hydrogen and/or oxygen as constituent elements. Elemental analysis gives information on the amount of C, N, H and S in the sample. Steam treated samples during 1.5 h and 15 h were measured after being treated in HCl (Table 2). From these analyses it can be seen that the quantity of hydrogen in the samples is negligible (<0.2 wt.%), indicating that no functional groups containing this element are present on the MWCNTs. The threshold of <0.2 wt.% used for hydrogen quantification is the same than that of N and S which are certainly not expected in these samples. Next, XPS

analysis was carried out to determine the presence/absence of oxygen in the steam treated samples. Integration of the high resolution spectra in the C1s and O1s regions (Figure S4) indicate similar levels of oxygen for as-received (1.3 % O/C) and steam treated samples for 1.5 h (1.0 % O/C) and 15 h (1.5 % O/C). It is therefore likely that such small levels of oxygen arise from the alumina impurities because the O/C ratio in the different samples follow the same trend than the alumina content as determined by TGA. Contribution from absorbed atmospheric species is also expected since the samples were exposed to atmospheric moisture and oxygen. Analysis of the C1s high resolution spectra allows the detection of different functional groups [54]. For instance, oxygen-bearing functionalities that could have been introduced during the treatment would be observed at binding energies below 290 eV. As it can be observed in Figure 7 there are no differences between the C1s peaks of as-made MWCNTs and the steam treated ones. Therefore, combining both XPS and elemental analysis we can conclude that no detectable functional groups are introduced in the MWCNT structure even after 15 h of steam exposure.

	at.% C	at.% H	at.% N	at.% S
Steam 1.5 h	97.79	<0.2	<0.2	<0.2
Steam 15 h	95.4	<0.2	<0.2	<0.2

Table 2. Amount of carbon, hydrogen, nitrogen, and sulfur obtained by elemental analysis of steam-treated samples for 1.5 h and 15 h (after HCl wash).

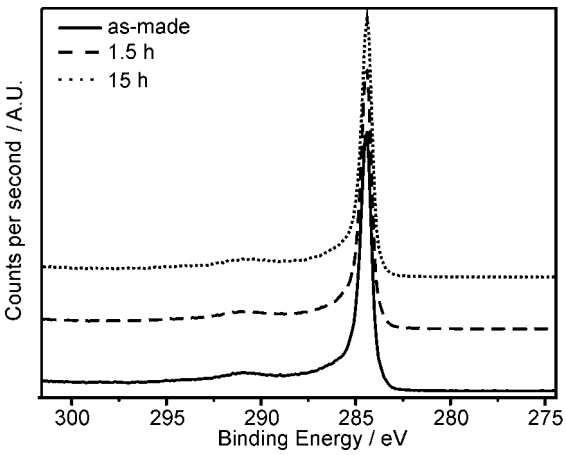

Figure 7. XPS spectra on the C 1s region of as-received MWCNTs and steam-purified MWCNTs during 1.5 h and 15 h. Spectra have been normalized for an ease of comparison.

Because no functionalities are detected either by XPS or by elemental analysis, we next performed Raman spectroscopy which provides information on the wall structure and purity of the MWCNTs. The two most prominent features in the Raman spectrum of MWCNTs are the G band arising at about 1575 cm^{-1}, which is related to well-ordered sp^2 graphite-type structures, and the D band centred at about 1341 cm^{-1}, which is commonly attributed to disordered sp^3-hybridized carbon material from defects and functionalities [55]. Beside those, in the Raman spectrum of MWCNTs it can be found a band at ~1620 cm^{-1} which appears as a shoulder on the G band and is denoted as D' band [56], a broad band at ~1200 cm^{-1} [57], and a band located between G and D band which is denoted as D" band [58]. Whereas the origin of D band can be attributed to both tube-related defects and amorphous carbon, D" band at ~1500 cm^{-1} originates only from the presence of amorphous carbon [58, 59]. Therefore, Choi et al. used intensity ratios of D" and G bands to estimate the purity of MWCNT samples [60]. It has been previously established that D" band has a Gaussian line shape [56, 58], in contrast to all the other aforementioned bands in Raman spectrum of MWCNT that have a Lorentzian

line shape.

Figure 8 displays Raman spectra of all the steam treated samples along with the as-received material. For the ease of inspection all the spectra are normalized to the G band intensity for both the green (514 nm; Fig. 6a) and red lasers (633 nm; Fig. 6b). Raman spectra measured with both laser for the as-received, 1.5 h and 15 h steam treated MWCNTs (followed by HCl wash) were fitted using four Lorentzian and one Gaussian component (Figure S5). The relative intensities of D and G bands are considered as probes of the CNT wall integrity and their degree of functionalization. The D/G intensity ratios derived from the fitted spectra are summarized in Figure 8c and Table S2. As expected, the D/G intensity ratio of a given sample is higher when measured at 633 nm than at 514 nm illustrating the dependence of this ratio on the laser excitation frequency [61]. An increase in the D/G intensity ratios can be observed for the steam treated samples which appears to be more pronounced at higher steam treatment times. As mentioned earlier, an increase in the D/G intensity ratios is typically attributed to disordered sp^3-hybridized carbon. From the analysis performed so far, it is clear that the functional groups present in the samples after the steam treatment are very limited. On the other hand, if side-wall defects were introduced onto the MWCNTs the reactivity of the resulting material with oxygen would be increased, and this is not the case according to TGA. Therefore, although side-wall defects cannot be discarded, it appears that the increase in the D/G intensity ratio is associated with the end-opening and shortening of the nanotubes. We advocate that MWCNTs oxidation takes place through the ends of the tubes, and, when opened, MWCNTs exhibit a higher amount of C sp^3. Moreover, this oxidation leads to a decrease of the CNT length during the treatment and an increase of the end-to-wall carbon ratio on the MWCNTs that gets reflected on the D-

band. To estimate the content of amorphous carbon in our samples, the D"/G ratios are presented in Figure 8d and summarized in Table S2. As it can be seen, for both Raman lasers D"/G ratios decrease for the steam treated samples compared to the as-received material. The decrease is more prominent when using the 633 nm Raman laser. Therefore, analysis of the Raman data also allows us to confirm that steam decreases the amount of amorphous carbon present in samples of as-received MWCNT.

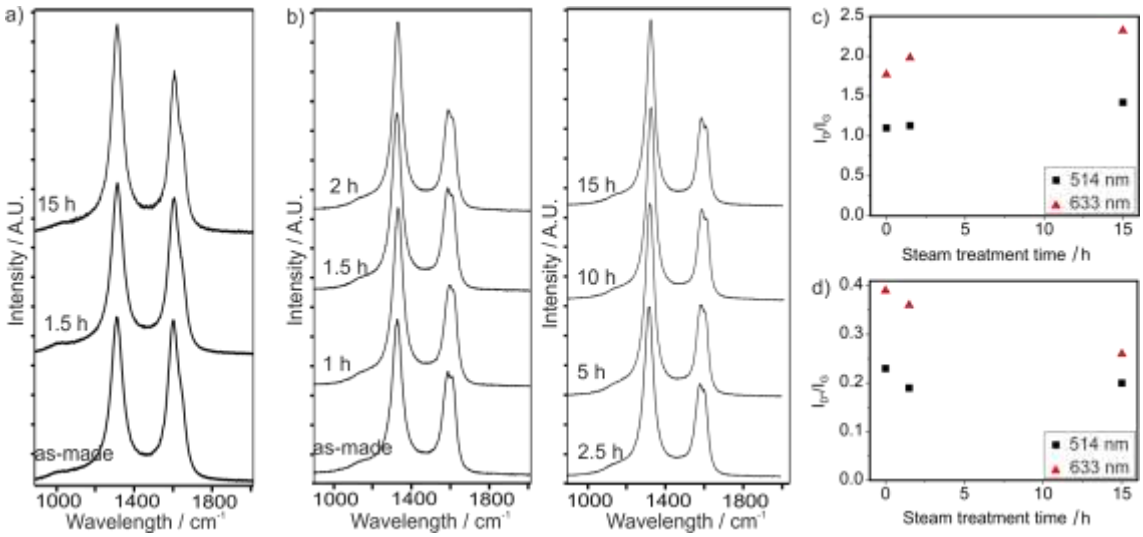

Figure 8. Raman spectra of as-made MWCNTs and steam-treated MWCNTs for different periods of time. a) Spectra obtained with green laser (514 nm). b) Spectra obtained with red laser (633 nm). c) Summary of the D/G band intensity ratio with respect of steam purification time for both lasers. d) Summary of the D"/G band intensity ratio with respect of steam purification time for both lasers.

To get further insight on this aspect, we analysed several individual MWCNTs by high resolution TEM (HRTEM) before and after a prolonged steam treatment. This technique allows the direct visualization of the carbon nanotube structure [62, 63] and provides information down to the atomic scale [64-66]. Figure 9 displays HRTEM images of a MWCNT from the as-received material where the walls are clearly visible, and a

MWCNT after a prolonged steam treatment (10 h). Albeit it is a long treatment, the MWCNT structure has been well preserved. The walls have no apparent breaks and the tubular structure remains intact. From a qualitative point of view the steam-treated MWCNTs have comparable structural integrity compared to as-received CNTs, which also natively contain defects (additional images are included in Figure S6). Therefore HRTEM confirms that the amount of defects introduced during the steam purification is sensibly low and that the observed increase in the D/G intensity ratio by Raman spectroscopy is most likely related to the end-opening and shortening of the MWCNTs.

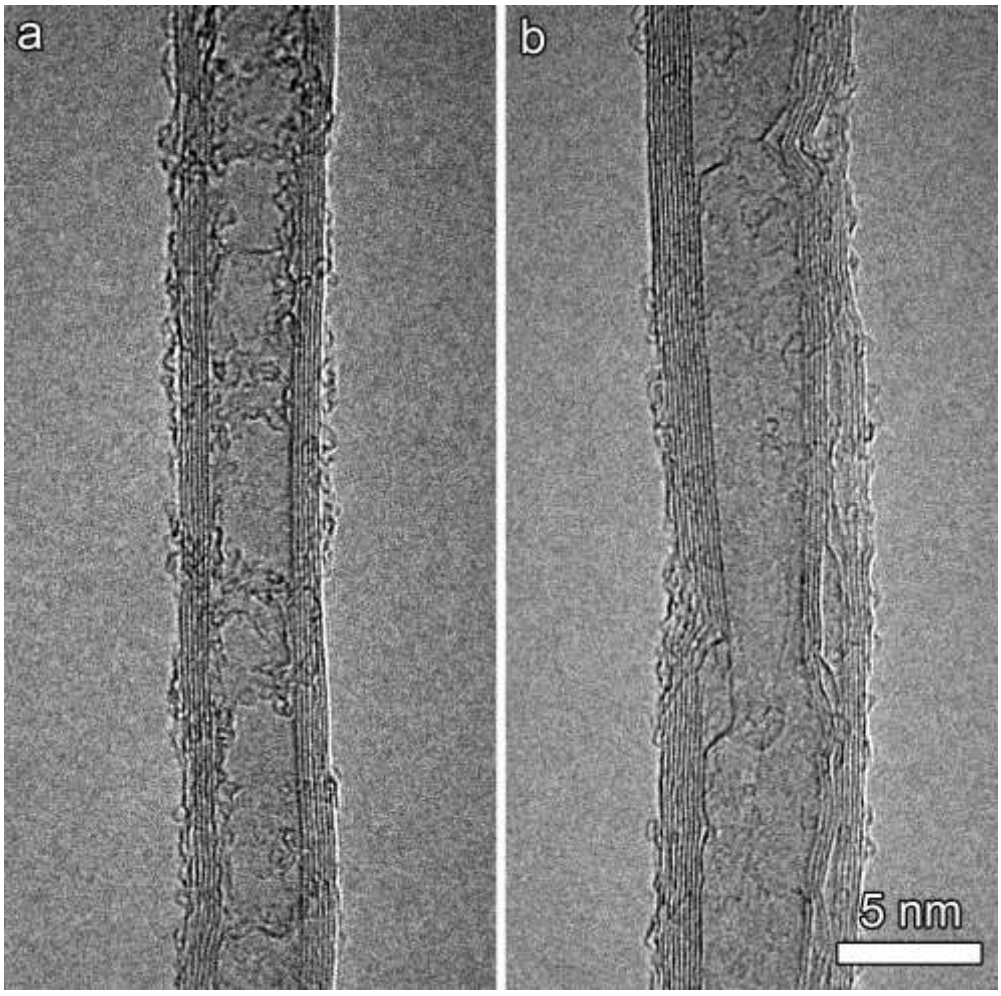

Figure 9. HRTEM images of a) as-received MWCNTs and b) Steam treated MWCNTs during 10 h.

4. Conclusions

We investigated the role that the steam treatment time plays on the purification, wall structure and length distribution of MWCNTs. Steam allows the removal of graphitic particles that sheath the metal catalysts (impurities from the CNTs' growth) and the amorphous carbon whilst reducing its impact on the wall structure of the MWCNTs. Oxygen- and hydrogen-bearing functionalities have not been detected on steam treated samples; neither by XPS nor by elemental analysis. Samples with a metal content below 0.01 wt% have been achieved by steam purification followed by an HCl wash. The steam purification treatment has been successfully achieved in both Fe-grown and CoMoCAT® MWCNTs. Steam is a simple, economic, and environmentally friendly method that results in end-opened high-quality nanotubes, the length of which can be easily modulated by a mere change of the treatment time. Open-ended CNTs with a low degree of functionalities are of interest for subsequent filling experiments since functional groups at the tips have been shown to block the entry ports of the nanochannels [67]. Therefore, steam further expands the toolbox of purification, end-opening and shortening strategies that allow the preparation of tailored MWCNT samples for selected applications.

Acknowledgements

The authors are grateful to Thomas Swan Co. & Ltd. for supplying the Elicarb® MWCNT samples. The research leading to these results has received funding from MINECO (MAT2011-24757) and the European Union Seventh Framework Programme under Grant Agreements 290023 - RADDEL (FP7-ITN) and 312483 - ESTEEM2 (Integrated Infrastructure Initiative-I3). L.C. acknowledges a JAE-Predoc fellowship (CSIC) and D.K. the financial support of the Ministry of Education, Science and

Technological Development of Republic of Serbia for postdoctoral research. This work was performed in the frame of the Materials Science PhD program of the Universitat Autònoma de Barcelona (L.C.). The XPS data was acquired at the Laboratorio de Microscopías Avanzadas (LMA) - Instituto de Nanociencia de Aragón (INA), EA at the Centres Científics i Tecnològics - Universitat de Barcelona, and TGA of CoMoCAT® MWCNTs at the Universitat d'Alacant, in Spain.

References

[1] Koyama S, Kim YA, Hayashi T, Takeuchi K, Fujii C, Kuroiwa N, et al. In vivo immunological toxicity in mice of carbon nanotubes with impurities. Carbon 2009;47(5):1365-72.

[2] Wörle-Knirsch JM, Pulskamp K, Krug HF. Oops They Did It Again! Carbon Nanotubes Hoax Scientists in Viability Assays. Nano Letters 2006;6(6):1261-8.

[3] Sharma H, Hussain S, Schlager J, Ali S, Sharma A. Influence of Nanoparticles on Blood–Brain Barrier Permeability and Brain Edema Formation in Rats. In: Czernicki Z, Baethmann A, Ito U, Katayama Y, Kuroiwa T, Mendelow D, eds. *Brain Edema XIV*: Springer Vienna 2010:359-64.

[4] Banks CE, Crossley A, Salter C, Wilkins SJ, Compton RG. Carbon Nanotubes Contain Metal Impurities Which Are Responsible for the "Electrocatalysis" Seen at Some Nanotube-Modified Electrodes. Angewandte Chemie International Edition 2006;45(16):2533-7.

[5] Henstridge MC, Shao L, Wildgoose GG, Compton RG, Tobias G, Green MLH. The Electrocatalytic Properties of Arc-MWCNTs and Associated 'Carbon Onions'. Electroanalysis 2008;20(5):498-506.

[6] Ambrosi A, Pumera M. Nanographite Impurities Dominate Electrochemistry of Carbon Nanotubes. Chemistry – A European Journal 2010;16(36):10946-9.

[7] Scott CL, Pumera M. Carbon nanotubes can exhibit negative effects in electroanalysis due to presence of nanographite impurities. Electrochemistry Communications 2011;13(5):426-8.

[8] An Z, Furmanchuk Ao, Ramachandramoorthy R, Filleter T, Roenbeck MR, Espinosa HD, et al. Inherent carbonaceous impurities on arc-discharge multiwalled carbon nanotubes and their implications for nanoscale interfaces. Carbon 2014;80(0):1-11.

[9] Shao L, Tobias G, Salzmann CG, Ballesteros B, Hong SY, Crossley A, et al. Removal of amorphous carbon for the efficient sidewall functionalisation of single-walled carbon nanotubes. Chemical Communications 2007;(47):5090-2.

[10] Ko FH, Lee CY, Ko CJ, Chu TC. Purification of multi-walled carbon nanotubes through microwave heating of nitric acid in a closed vessel. Carbon 2005;43(4):727-33.

[11] Chen XH, Chen CS, Chen Q, Cheng FQ, Zhang G, Chen ZZ. Non-destructive purification of multi-walled carbon nanotubes produced by catalyzed CVD. Materials Letters 2002;57(3):734-8.

[12] Feng Y, Zhang H, Hou Y, McNicholas TP, Yuan D, Yang S, et al. Room temperature purification of few-walled carbon nanotubes with high yield. ACS Nano 2008;2(8):1634-8.

[13] Yuan JM, Chen XH, Fan ZF, Yang XG, Chen ZH. An easy method for purifying multi-walled carbon nanotubes by chlorine oxidation. Carbon 2008;46(9):1266-9.

[14] Ming J, Wu Y, Yu Y, Zhao F. Steaming multiwalled carbon nanotubesvia acid vapour for controllable nanoengineering and the fabrication of carbon nanoflutes. Chemical Communications 2011;47(18):5223-5.

[15] Suri A, Coleman KS. The superiority of air oxidation over liquid-phase oxidative treatment in the purification of carbon nanotubes. Carbon 2011;49(9):3031-8.

[16] Ebbesen TW, Ajayan PM, Hiura H, Tanigaki K. Purification of nanotubes. Nature 1994;367(6463):519-.

[17] Tobias G, Shao L, Salzmann CG, Huh Y, Green MLH. Purification and Opening of Carbon Nanotubes Using Steam. The Journal of Physical Chemistry B 2006;110(45):22318-22.

[18] Babu DJ, Yadav S, Heinlein T, Cherkashinin G, Schneider JJ. Carbon Dioxide Plasma as a Versatile Medium for Purification and Functionalization of Vertically Aligned Carbon Nanotubes. The Journal of Physical Chemistry C 2014;118(22):12028-34.

[19] Chng ELK, Poh HL, Sofer Z, Pumera M. Purification of carbon nanotubes by high temperature chlorine gas treatment. Physical Chemistry Chemical Physics 2013;15(15):5615-9.

[20] Vivekchand SRC, Govindaraj A, Seikh MM, Rao CNR. New Method of Purification of Carbon Nanotubes Based on Hydrogen Treatment. The Journal of Physical Chemistry B 2004;108(22):6935-7.

[21] Meyer-Plath A, Orts-Gil G, Petrov S, Oleszak F, Maneck H-E, Dörfel I, et al. Plasma-thermal purification and annealing of carbon nanotubes. Carbon 2012;50(10):3934-42.

[22] Wiltshire JG, Khlobystov AN, Li LJ, Lyapin SG, Briggs GAD, Nicholas RJ. Comparative studies on acid and thermal based selective purification of HiPCO produced single-walled carbon nanotubes. Chemical Physics Letters 2004;386(4–6):239-43.

[23] Ballesteros B, Tobias G, Shao L, Pellicer E, Nogués J, Mendoza E, et al. Steam Purification for the Removal of Graphitic Shells Coating Catalytic Particles and the Shortening of Single-Walled Carbon Nanotubes. Small 2008;4(9):1501-6.

[24] Guo W, Dou Z, Li H, Shi Z, Sun H, Liu Y. An efficient strategy for the purification of cloth-like single walled carbon nanotube soot produced by arc discharge. Carbon 2010;48(13):3769-77.

[25] Xia W, Hagen V, Kundu S, Wang Y, Somsen C, Eggeler G, et al. Controlled Etching of Carbon Nanotubes by Iron-Catalyzed Steam Gasification. Advanced Materials 2007;19(21):3648-52.

[26] Ponrouch A, Palacín MR. Optimisation of performance through electrode formulation in conversion materials for lithium ion batteries: Co3O4 as a case example. Journal of Power Sources 2012;212(0):233-46.

[27] Mendoza-Sánchez B, Rasche B, Nicolosi V, Grant PS. Scaleable ultra-thin and high power density graphene electrochemical capacitor electrodes manufactured by aqueous exfoliation and spray deposition. Carbon 2013;52(0):337-46.

[28] Huang C, Grobert N, Watt AAR, Johnston C, Crossley A, Young NP, et al. Layer-by-layer spray deposition and unzipping of single-wall carbon nanotube-based thin film electrodes for electrochemical capacitors. Carbon 2013;61(0):525-36.

[29] Chu BTT, Tobias G, Salzmann CG, Ballesteros B, Grobert N, Todd RI, et al. Fabrication of carbon-nanotube-reinforced glass-ceramic nanocomposites by ultrasonic in situ sol-gel processing. Journal of Materials Chemistry 2008;18(44):5344-9.

[30] Cabana L, Ballesteros B, Batista E, Magén C, Arenal R, Oró-Solé J, et al. Synthesis of PbI_2 Single-Layered Inorganic Nanotubes Encapsulated Within Carbon Nanotubes. Advanced Materials 2014;26(13):2016-21.

[31] Pascu SI, Arrowsmith RL, Bayly SR, Brayshaw S, Hu Z. Towards nanomedicines: design protocols to assemble, visualize and test carbon nanotube probes for multi-modality biomedical imaging. Philosophical Transactions of the Royal Society A: Mathematical, Physical and Engineering Sciences 2010;368(1924):3683-712.

[32] Wang JT-W, Cabana L, Bourgognon M, Kafa H, Protti A, Venner K, et al. Magnetically Decorated Multiwalled Carbon Nanotubes as Dual MRI and SPECT Contrast Agents. Advanced Functional Materials 2014;24(13):1880-94.

[33] Heister E, Brunner EW, Dieckmann GR, Jurewicz I, Dalton AB. Are Carbon Nanotubes a Natural Solution? Applications in Biology and Medicine. ACS Applied Materials & Interfaces 2013;5(6):1870-91.

[34] Tobias G, Martincic M. Filled carbon nanotubes in biomedical imaging and drug delivery. Expert Opinion on Drug Delivery 2015;12:563-81.

[35] Zhang X, Jiao K, Wang X. Paste Electrode Based on Short Single-Walled Carbon Nanotubes and Room Temperature Ionic Liquid: Preparation, Characterization and Application in DNA Detection. Electroanalysis 2008;20(12):1361-6.

[36] Fonseca A, Reijerkerk S, Potreck J, Nijmeijer K, Mekhalif Z, Delhalle J. Very short functionalized carbon nanotubes for membrane applications. Desalination 2010;250(3):1150-4.

[37] Wang X, Wang J, Chang H, Zhang Y. Preparation of Short Carbon Nanotubes and Application as an Electrode Material in Li-Ion Batteries. Advanced Functional Materials 2007;17(17):3613-8.

[38] Kim YA, Hayashi T, Fukai Y, Endo M, Yanagisawa T, Dresselhaus MS. Effect of ball milling on morphology of cup-stacked carbon nanotubes. Chemical Physics Letters 2002;355(3–4):279-84.

[39] Lustig SR, Boyes ED, French RH, Gierke TD, Harmer MA, Hietpas PB, et al. Lithographically Cut Single-Walled Carbon Nanotubes: Controlling Length Distribution and Introducing End-Group Functionality. Nano Letters 2003;3(8):1007-12.

[40] Gu Z, Peng H, Hauge RH, Smalley RE, Margrave JL. Cutting Single-Wall Carbon Nanotubes through Fluorination. Nano Letters 2002;2(9):1009-13.

[41] Marega R, Accorsi G, Meneghetti M, Parisini A, Prato M, Bonifazi D. Cap removal and shortening of double-walled and very-thin multi-walled carbon nanotubes under mild oxidative conditions. Carbon 2009;47(3):675-82.

[42] Hata K, Futaba DN, Mizuno K, Namai T, Yumura M, Iijima S. Water-Assisted Highly Efficient Synthesis of Impurity-Free Single-Walled Carbon Nanotubes. Science 2004;306(5700):1362-4.

[43] Yamada T, Maigne A, Yudasaka M, Mizuno K, Futaba DN, Yumura M, et al. Revealing the Secret of Water-Assisted Carbon Nanotube Synthesis by Microscopic Observation of the Interaction of Water on the Catalysts. Nano Letters 2008;8(12):4288-92.

[44] Amama PB, Pint CL, McJilton L, Kim SM, Stach EA, Murray PT, et al. Role of water in super growth of single-walled carbon nanotube carpets. Nano Letters 2009;9(1):44-9.

[45] Kolodiazhnyi T, Pumera M. Towards an Ultrasensitive Method for the Determination of Metal Impurities in Carbon Nanotubes. Small 2008;4(9):1476-84.

[46] Cornell R, Schwertmann U. The Iron Oxides: Structure, Properties, Reactions, Occurences and Uses: Wiley-VCH 2004.

[47] Xavier B, Amílcar L. Finite-size effects in fine particles: magnetic and transport properties. Journal of Physics D: Applied Physics 2002;35(6):R15.

[48] Pumera M. Carbon Nanotubes Contain Residual Metal Catalyst Nanoparticles even after Washing with Nitric Acid at Elevated Temperature Because These Metal Nanoparticles Are Sheathed by Several Graphene Sheets. Langmuir 2007;23(11):6453-8.

[49] Chiang IW, Brinson BE, Smalley RE, Margrave JL, Hauge RH. Purification and Characterization of Single-Wall Carbon Nanotubes. The Journal of Physical Chemistry B 2001;105(6):1157-61.

[50] Ballesteros B, Tobias G, Ward MAH, Green MLH. Quantitative Assessment of the Amount of Material Encapsulated in Filled Carbon Nanotubes. The Journal of Physical Chemistry C 2009;113(7):2653-6.

[51] Brukh R, Mitra S. Kinetics of carbon nanotube oxidation. Journal of Materials Chemistry 2007;17(7):619-23.

[52] Shuba MV, Paddubskaya AG, Kuzhir PP, Maksimenko SA, Ksenevich VK, Niaura G, et al. Soft cutting of single-wall carbon nanotubes by low temperature ultrasonication in a mixture of sulfuric and nitric acids. Nanotechnology 2012;23(49):495714.

[53] Rubio N, Fabbro C, Herrero MA, de la Hoz A, Meneghetti M, Fierro JLG, et al. Ball-Milling Modification of Single-Walled Carbon Nanotubes: Purification, Cutting, and Functionalization. Small 2011;7(5):665-74.

[54] T.I.T. Okpalugo, P. Papakonstantinou, H. Murphy, J. McLaughlin, Brown NMD. High resolution XPS characterization of chemical functionalised MWCNTs and SWCNTs. Carbon 2005;43:153-61.

[55] Kim UJ, Furtado CA, Liu X, Chen G, Eklund PC. Raman and IR Spectroscopy of Chemically Processed Single-Walled Carbon Nanotubes. Journal of the American Chemical Society 2005;127(44):15437-45.

[56] Sadezky A, Muckenhuber H, Grothe H, Niessner R, Pöschl U. Raman microspectroscopy of soot and related carbonaceous materials: Spectral analysis and structural information. Carbon 2005;43(8):1731-42.

[57] Schwan J, Ulrich S, Batori V, Ehrhardt H, Silva SRP. Raman spectroscopy on amorphous carbon films. Journal of Applied Physics 1996;80(1):440-7.

[58] Jawhari T, Roid A, Casado J. Raman spectroscopic characterization of some commercially available carbon black materials. Carbon 1995;33(11):1561-5.

[59] Cuesta A, Dhamelincourt P, Laureyns J, Martínez-Alonso A, Tascón JMD. Raman microprobe studies on carbon materials. Carbon 1994;32(8):1523-32.

[60] Choi YC, Min K-I, Jeong MS. Novel Method of Evaluating the Purity of Multiwall Carbon Nanotubes Using Raman Spectroscopy. Journal of Nanomaterials 2013;2013:6.

[61] Brown SDM, Jorio A, Dresselhaus MS, Dresselhaus G. Observations of the D-band feature in the Raman spectra of carbon nanotubes. Physical Review B 2001;64(7):073403.

[62] Suarez-Martinez I, Ewels CP, Ke X, Van Tendeloo G, Thiess S, Drube W, et al. Study of the Interface between Rhodium and Carbon Nanotubes. ACS Nano 2010;4(3):1680-6.

[63] Felten A, Gillon X, Gulas M, Pireaux J-J, Ke X, Van Tendeloo G, et al. Measuring Point Defect Density in Individual Carbon Nanotubes Using Polarization-Dependent X-ray Microscopy. ACS Nano 2010;4(8):4431-6.

[64] Börrnert F, Gorantla S, Bachmatiuk A, Warner JH, Ibrahim I, Thomas J, et al. In situ observations of self-repairing single-walled carbon nanotubes. Physical Review B 2010;81(20):201401.

[65] Allen CS, Robertson AW, Kirkland AI, Warner JH. The Identification of Inner Tube Defects in Double-Wall Carbon Nanotubes. Small 2012;8(24):3810-5.

[66] Hong SY, Tobias G, Ballesteros B, El Oualid F, Errey JC, Doores KJ, et al. Atomic-Scale Detection of Organic Molecules Coupled to Single-Walled Carbon Nanotubes. Journal of the American Chemical Society 2007;129(36):10966-7.

[67] Kuznetsova A, Mawhinney DB, Naumenko V, Yates Jr JT, Liu J, Smalley RE. Enhancement of adsorption inside of single-walled nanotubes: opening the entry ports. Chemical Physics Letters 2000;321(3–4):292-6.